Medical Physics
The International Journal of Medical Physics Research and Practice

3D calculation of radiation-induced second cancer risk including dose and tissue response heterogeneities

C. Timlin, D. R. Warren, B. Rowland, A. Madkhali, J. Loken, M. Partridge, B. Jones, J. Kruse, and R. Miller

Citation: Medical Physics **42**, 866 (2015); doi: 10.1118/1.4905158
View online: http://dx.doi.org/10.1118/1.4905158
View Table of Contents: http://scitation.aip.org/content/aapm/journal/medphys/42/2?ver=pdfcov
Published by the American Association of Physicists in Medicine

3D calculation of radiation-induced second cancer risk including dose and tissue response heterogeneities

C. Timlin,[a] D. R. Warren, B. Rowland, A. Madkhali, and J. Loken
Particle Therapy Cancer Research Institute, University of Oxford, Oxfordshire OX1 3RH, United Kingdom and Department of Physics, University of Oxford, Oxfordshire OX1 3RH, United Kingdom

M. Partridge and B. Jones
CRUK/MRC Oxford Institute for Radiation Oncology, Department of Oncology, University of Oxford, Oxford OX3 7DQ, United Kingdom

J. Kruse and R. Miller
Mayo Clinic, Rochester, Minnesota 55905

(Received 3 April 2014; revised 5 December 2014; accepted for publication 8 December 2014; published 26 January 2015)

Purpose: Tools for comparing relative induced second cancer risk, to inform choice of radiotherapy treatment plan, are becoming increasingly necessary as the availability of new treatment modalities expands. Uncertainties, in both radiobiological models and model parameters, limit the confidence of such calculations. The aim of this study was to develop and demonstrate a software tool to produce a malignant induction probability (MIP) calculation which incorporates patient-specific dose and allows for the varying responses of different tissue types to radiation.
Methods: The tool has been used to calculate relative MIPs for four different treatment plans targeting a subtotally resected meningioma: 3D conformal radiotherapy (3DCFRT), volumetric modulated arc therapy (VMAT), intensity-modulated x-ray therapy (IMRT), and scanned protons.
Results: Two plausible MIP models, with considerably different dose–response relationships, were considered. A fractionated linear–quadratic induction and cell-kill model gave a mean relative cancer risk (normalized to 3DCFRT) of 113% for VMAT, 16% for protons, and 52% for IMRT. For a linear no-threshold model, these figures were 105%, 42%, and 78%, respectively. The relative MIP between plans was shown to be significantly more robust to radiobiological parameter uncertainties compared to absolute MIP. Both models resulted in the same ranking of modalities, in terms of MIP, for this clinical case.
Conclusions: The results demonstrate that relative MIP is a useful metric with which treatment plans can be ranked, regardless of parameter- and model-based uncertainties. With further validation, this metric could be used to discriminate between plans that are equivalent with respect to other planning priorities. [http://dx.doi.org/10.1118/1.4905158]

Key words: radiation-induced cancer, proton therapy, radiotherapy

1. INTRODUCTION

Recent advances in radiotherapy techniques have resulted in a wide array of treatment modalities, more than one of which may be considered for a given patient/class of patients. Modern techniques such as intensity-modulated x-ray therapy (IMRT) and volumetric modulated arc therapy (VMAT) produce high-dose regions which conform closely to the target volume. However, this is generally achieved by substantially increasing the volume of normal tissue exposed to a low dose, and concern has been expressed that this might in some cases enhance the ongoing health risks to the patient.[1]

Clinically, a set of established dose constraints (designed to couple a high tumor control probability, TCP, with a low normal tissue complication probability, NTCP) can often be met by a number of treatment plans, potentially spanning several different radiotherapy modalities. These plans may be considered equivalent with regards to cure probability and severe acute and late radiation toxicity to normal tissues, so it then becomes prudent to consider additional factors which might allow discrimination between the various options such as the induction of secondary malignancies by radiotherapy.

The lag time in the appearance of secondary tumors after radiotherapy is dependent on the individual tumor type but is usually greater than a decade for solid tumors.[2] The number of cancer diagnoses is rising year-on-year, while life expectancy post-treatment has increased at the same time.[3] Consequently, it is more important than ever to consider the long-term effects of treatment.

Radiation therapy gives rise to premalignant initiated cells when DNA damage is misrepaired, leading to mutations in the genetic code. Some of this damage can cause a full malignancy over time, for example, by impairing the function of tumor suppressor genes.[4] The mechanism whereby an ordinary cell gives rise to malignant cells is a complex, multistage process. However, it is widely accepted that it can

be described fairly well by three steps: initiation, promotion, and progression.[5,6] The first step is the conversion of normal tissue stem cells into "initiated" cells, generally by a genetic mutation.[4] These initiated cells are premalignant, and will not develop into a tumor directly, but may achieve some growth advantages in the presence of various "promoter" risk factors (cigarette smoking being a well known example) or conversely in the absence of suppressors.[7] Subsequent events can then cause these cells to "progress" into a fully malignant state, displaying the essential characteristics of cancerous growth "self-sufficiency in growth signals, insensitivity to growth-inhibitory (antigrowth) signals, evasion of programmed cell death (apoptosis), limitless replicative potential, sustained angiogenesis, and tissue invasion and metastasis."[8]

However, research to date indicates that radiotherapy only makes an appreciable contribution to the first stage in this sequence, the production of initiated cells.[9] It is therefore assumed that calculation of radiation-induced secondary cancer risk can be based on initiation alone, and that the overall probability of secondary tumors will vary linearly with the number of initiated cells present in the patient.[10] The constant of proportionality will be a nontrivial function of many parameters such as patient age and general state of health, as well as exposure to environmental promoting factors, but is assumed to be independent of any properties of the radiotherapy treatment. The clinical example used as an illustration in this paper therefore compares multiple plans for the same patient in order to deconvolute the induction from promotion and progression.[11]

While atomic bomb data have established a linear relationship between cancer incidence and dose in the region from about 5 cGy to 2.5 Gy,[12] there is still great debate as to how this relationship can be extrapolated to model radiation-induced second cancers at therapeutic doses. A number of clinical and epidemiological studies report on second cancer occurrences following radiotherapy,[13–16] with dose–response relationships being most recently reviewed by de Gonzalez and coauthors in 2012.[17] In brief, the shape of the dose–response curve seemingly varies between induced cancer types, but most existing individual studies do not have sufficient statistics to characterize it with any degree of certainty. Nevertheless, monotonic increases in second cancer risk (with or without a plateau) seem likely, but not conclusively proven, in the therapeutic dose regime for most second cancer sites considered by the aforementioned review (breast, brain, lung, and bone). However, a study with relatively good statistics does suggest a turnover in the induction of thyroid cancer,[18] and preclinical studies have shown a similarly shaped curve for cancer induction in mice.[19,20] The radiobiological models used as illustration in this paper are intended to represent lower and upper bounds for the actual dose–response relationship for cell initiation. The models do not explicitly include either promotion or progression, which are assumed to be broadly independent of radiation exposure, or repopulation. It should be noted that incorporating repopulation of premalignant cells can lead to dose–response curves that plateau at high doses even if the individual cell induction probabilities exhibit a turnover.[21]

This paper details a method to calculate malignant induction probability (MIP) by considering the expected number of transformed cells in each voxel of the treatment volume. In doing so it follows the requirement, as previously identified by others,[22] for both dose and tissue heterogeneities to be taken into account. Confidence in second cancer risk estimates is limited by uncertainty in the most appropriate radiobiological model and parameters. It is necessary to quantify the magnitude of the error in risk introduced by these input uncertainties. Therefore, in this work, each tissue type is associated with a set of mean radiobiological input parameters which are allowed to vary around this mean. Thus, the sensitivity of the MIP calculation to changes in input parameters is estimated. Two plausible models for the probability of initiation of premalignant cells are employed with considerably different dose–response relationships. Finally, the functionality of the method is demonstrated by comparing MIP for four different treatment plans for an example patient with a subtotally resected meningioma.

2. METHODS

2.A. Linear–quadratic–exponential (LQE) model

2.A.1. Single fraction transformation probability

The probability of a cell becoming transformed/initiated (P_T) when exposed to a single dose of radiation, d, can be modeled as linear–quadratic (LQ) with the delivered dose

$$P_{T_{\mathrm{LQ}}}(d) = \gamma d + \delta d^2. \tag{1}$$

Initiated cells will also have a probability of being killed by radiation, which increases with dose. A transformed cell will have to survive if it is to be deemed a threat. Therefore, the transformation probability can be expressed as the product of Eq. (1) and the probability of cell survival, leading to the "linear–quadratic–exponential" (LQE) expression for the probability of transformation and survival,

$$P_{TS_{\mathrm{LQE}}}(d) = P_{T_{\mathrm{LQ}}}(d) P_S(d) \tag{2}$$

$$= (\gamma d + \delta d^2) e^{-(\alpha d + \beta d^2)}. \tag{3}$$

γ and δ are the coefficients for the linear and dose-squared terms of cancer induction and P_S is the surviving fraction, which is a function of the linear–quadratic radiosensitivity parameters α and β.[23]

2.A.2. Fractionation effects

It is important that the effect of fractionation is included when deriving an expression for surviving and transformed cells after clinical radiation treatment. While an approximation for the fractionated probability has been cited elsewhere in the literature,[24–26] here the full functional form is derived. For this a 3-pool model, detailed graphically in Fig. 1, is employed. The model shows how the state of an initially living cell may evolve after two fractions have been delivered. After each fraction of

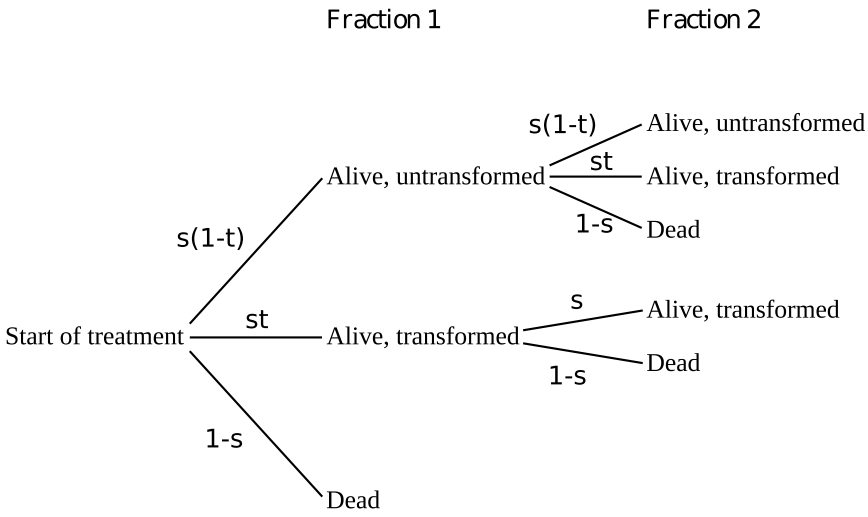

FIG. 1. A probability tree showing how the state of a cell evolves with each radiotherapy fraction. The possible states are dead; alive and transformed or alive and untransformed. The probability that a cell survives a single fraction is s [shorthand for $P_S(d)$] and the probability that those surviving cells undergo premalignant transformation is t [shorthand for $P_T(d)$]. Two fractions are shown here, the generalized expression for n fractions is shown in Eq. (4) and derived in Appendix.

radiation, followed by 24 h repair, the cell is considered to be in 1 of 3 states:

- Surviving and normal (untransformed),
- Surviving and transformed,
- Dead/sterilized.

This can be generalized (as shown in Appendix) to produce the probability that a cell will be transformed and survives after n fractions of radiation

$$P_{TS}(n,d) = s^n(1-(1-t)^n), \tag{4}$$

where the shorthands $s = P_S(d)$ and $t = P_T(d)$ have been used. When t is much less than 1, it is sufficient to expand binomially the bracket in the second term to first order only as demonstrated in Appendix giving

$$P_{TS}(n,d) \approx nP_T(d)P_S(d)^n. \tag{5}$$

This fractionated model for linear–quadratic transformation and survival is employed on a voxel-by-voxel basis in the software tool and is hereafter referred to as the LQE model.

2.B. Linear model

A linear no-threshold dose–response model is widely used to estimate the occupational risk for malignant induction at low dose and low dose rates.[27] Sachs and Brenner have demonstrated that after the inclusion of repopulation in models such as the LQE, "the number of radiation associated premalignant stem cells present after repopulation has ceased is essentially linear in dose" for doses below about 5 Gy.[10] A model that extrapolates this linearity to higher doses can be considered an upper bound on dose–response, with models that tend to zero as dose approaches infinity (such as the LQE) constituting a lower bound and models that plateau at high doses lying in-between.

The mathematical form of this "linear" dose–response model is simply

$$P_{TS_L}(d) = \gamma D, \tag{6}$$

where D is the total dose, equivalent to the dose per fraction (d) multiplied by the number of fractions (n) and γ is the malignant transformation coefficient.

This linear model has no low-dose threshold for induction of malignancy, as suggested by the Life Span Study data.[28]

2.C. Applying the models to treatment plans

A novel software framework has been developed to evaluate a voxelized calculation for the risk of second cancer for a given radiotherapy treatment plan (Fig. 2). It is written using MATLAB (Ref. 29) and employs some functionality from computational environment for radiation research (CERR).[30] When fully validated, it is intended to be of use during the treatment planning process by providing the clinician with additional information with which to discriminate between different plans and treatment modalities. The framework is designed to operate on plans in the DICOM-RT format importing planning CT, structure sets, and dose cubes.

The first stage in the process uses functions from the CERR platform to import the structures and doses and extract the necessary data. Where a voxel has more than one tissue flag, the software is designed to select the most specific structure, such that all voxels within the patient are assigned to precisely one structure. For example, the lens is a substructure within the eye, so voxels within this contour will be labeled "lens" instead of "eye." The resulting structure matrix is used to assign radiobiological parameters to each voxel via a look-up table. A corresponding dose map is then calculated on the same voxel grid by linear interpolation of the DICOM-RT dose description.

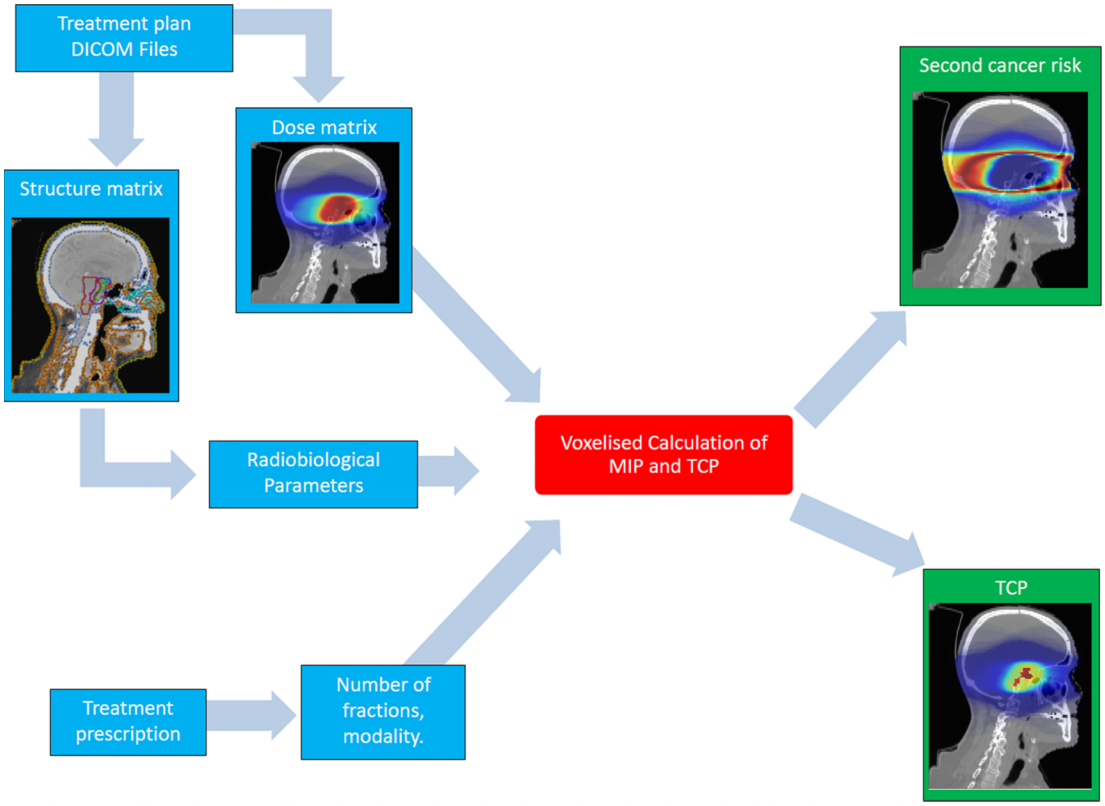

FIG. 2. A schematic showing the main inputs and outputs of the treatment outcome modeling software. A job management database, not shown here, produces 1000 sets of input parameters in a Monte Carlo fashion which are applied to each treatment plan. Output distributions of MIP and TCP for each treatment plan are then calculated.

2.C.1. Voxel-by-voxel calculations

Once the radiobiological parameters (α, β, γ, and δ) and dose have been assigned to each voxel, the expected number of cells transformed in that voxel is calculated. This is also dependent on the number of fractions the treatment is delivered in. The expected number of transformed cells remaining post-treatment, in each voxel in the treatment volume, can be expressed as

$$C_{TSi_{\mathrm{LQE}}} = C_{0i} n \left(\gamma_i d_i + \delta_i d_i^2\right) e^{-n\left(\alpha_i d_i + \beta_i d_i^2\right)} \tag{7}$$

for the LQE model, where C_{0i} is the number of cells pretreatment in voxel i, and

$$C_{TSi_{\mathrm{L}}} = C_{0i} n \gamma_i d_i \tag{8}$$

for the linear model.

Dose per fraction, d_i, is the dose in voxel i of the interpolated dose map, divided by the number of fractions. Proton treatments are currently planned assuming that relative biological effectiveness (RBE) is 1.1 for all voxels. The dose matrix can therefore be incorporated in the same way as the photon plans, because it is essentially equivalent to planned dose multiplied by RBE.

2.C.2. Integrated second cancer risk calculation

MIP, defined as "the risk of inducing one or more secondary cancers," can be calculated by integrating the C_{TS} results for each voxel over the whole treatment volume. The assumption is made that radiation-induced secondary cancer risk is directly proportional to the number of initiated cells present in the patient after treatment, as described in Sec. 1. The constant of proportionality, hereafter denoted by ϵ, is the probability that a transformed premalignant cell develops into an overt malignancy. MIP can be expressed as $1 - R_0$ (where R_0 is probability that the treatment induces zero cancers). Assuming a Poisson distribution for the number of transformed cells,

$$\mathrm{MIP} = 1 - R_0 = 1 - e^{-\epsilon \sum_{i=1}^{N} C_{TSi}}, \tag{9}$$

where N is the total number of voxels that make up the treatment volume.

In the limit that the exponent is much smaller than 1, MIP $\approx \epsilon \sum_{i=1}^{N} C_{TSi}$, thus choosing the LQE model for malignant induction yields

$$\mathrm{MIP}_{\mathrm{LQE}} \approx \epsilon\, n \sum_{i=1}^{N} C_{0i} \left(\gamma_i d_i + \delta_i d_i^2\right) e^{-n\left(\alpha_i d_i + \beta_i d_i^2\right)} \tag{10}$$

and substituting the linear model gives

$$\mathrm{MIP}_{L} \approx \epsilon\, n \sum_{i=1}^{N} C_{0i} \gamma_i d_i. \tag{11}$$

Relative MIP (RelMIP) is defined as the ratio of MIP for two given treatment plans. It is assumed that ϵ [Eq. (9)] is a patient-specific quantity and therefore cancels when

comparing two given treatment plans on the same patient,[31]

$$\text{RelMIP} \approx \frac{\sum_{i=1}^{N} C_{TSi}^{\text{Plan1}}}{\sum_{i=1}^{N} C_{TSi}^{\text{Plan2}}}. \quad (12)$$

In Sec. 2.C.4, a specific clinical example will be used to demonstrate the utility of RelMIP in ranking treatment plans.

2.C.3. Sensitivity of MIP to parameter uncertainty

Calculations of initiated cell creation involve several radiobiological parameters whose values are not always well defined. To quantify the effect of parameter uncertainty on the outcome metrics, the software framework has been designed to run multiple jobs in parallel which span a range of input parameter values. The job management system uses a Monte Carlo approach, selecting a set of parameters by randomly sampling a normal distribution about each parameter's average value as shown in Fig. 3. The resulting set of parameters is then applied to all voxels in all plans being considered and used to calculate integrated radiobiological endpoints such as MIP, RelMIP, and TCP for each plan.

2.C.4. Clinical example—subtotally resected meningioma

The functionality of the software framework is demonstrated by applying it to the case of a patient with subtotally resected atypical meningioma. The Varian Eclipse planning system was used to plan radiotherapy treatments with scanned protons and three photon modalities: IMRT, VMAT, and 3D conformal radiotherapy (3DCFRT). All modalities were planned using the same set of dose constraints for both the PTV and organs at risk (detailed in Table I), which were the Mayo Clinic's standard values for tumors of the brain at the time of treatment planning. The PTV prescription dose was 50.4 Gy in 28 fractions. More information about the dose–volume characteristics of the four plans is detailed in Table II.

The 3DCFRT plan consisted of two coplanar opposed laterals, a noncoplanar vertex field and an anterior–superior angled noncoplanar beam; the VMAT plan consisted of two noncoplanar arcs; the IMRT plan consisted of multiple coplanar beams; and the proton plan consisted of two coplanar beams. It should be noted that the planned dose, and any metrics (such as MIP) derived from it, is specific to each plan with the specified set of beam arrangements. The plans are not necessarily indicative of the modality as a whole. Employing different beam arrangements could lead to notably different results for MIP, especially if the integrated volume receiving nonzero dose changes appreciably.

The set of radiobiological parameters used in this example are given in Table III. Mean values for parameters were calculated using published α/β ratios for normal tissue,[32] with the assumption that $\bar{\beta} = 0.03$ Gy^{-2}. For the tumor volume, $\bar{\alpha} = 0.15$ Gy^{-1}.[33] Because of the lack of available data on values for γ and δ, these parameters must be estimated. The mechanism of cell transformation is presumed to be similar to that for cell kill, such that the γ/δ ratios required in the LQE model are the same as α/β ratios, with the scaling constant chosen so that $\bar{\gamma}/\bar{\alpha} = 10^{-6}$. The product of $\bar{\gamma}/\bar{\alpha}$ and ϵ (the probability that a transformed cell becomes an overt malignancy) has been chosen to give final MIP estimates of approximately 10% for a conventional x-ray plan, which is comparable to lifetime risks observed in other studies of cranial irradiation.[34,35] It should be noted that RelMIP [Eq. (12)] is independent of both ϵ and the scale factor linking $\bar{\gamma}$ to $\bar{\alpha}$. The number of clonogens within the GTV contour was calculated on the premise that a TCP of about 95% would be expected for a resected meningioma treated to this dose.

Given this set of mean values, a parameter set for each run was calculated using Gaussian distributions with a coefficient of variation (σ/μ) of 10%. Each parameter set was then applied to all four treatment plans simultaneously, and a total of 1000 individual sets were used to create probability distributions for MIP_L, MIP_LQE, and TCP. The 3DCFRT distribution was chosen as a baseline for RelMIP_L and RelMIP_LQE comparison.

3. RESULTS

3.A. Voxel-by-voxel calculation

Figure 4 shows 2D voxel maps of dose, surviving fraction, and cells transformed for the IMRT and proton treatment plans. These images illustrate some important features of modeling biological endpoints on a voxel-by-voxel basis. The surviving fraction of cells is not constant over the treatment volume, despite uniform dose, as it depends on the tissues' sensitivity to radiation. This biologically heterogeneous response results in lower surviving fraction of clonogenic cells in the tumor region than in the surrounding normal tissue. This is demonstrated by

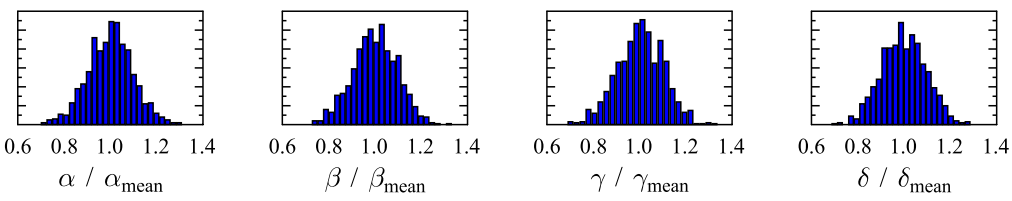

FIG. 3. Histograms showing the distribution of four radiobiological input parameters α, β, γ, and δ (scaled to their mean values) chosen for a typical sensitivity analysis. The height of each bar relates to the number of code runs in that bin range. Each parameter set is chosen in a Monte Carlo fashion by randomly sampling a normal distribution for each parameter with a given mean and standard deviation. MIP is then calculated for each individual parameter set to attain a MIP distribution and assess the sensitivity to input uncertainty.

TABLE I. Planning priorities for subtotally resected atypical meningioma. These parameters, used at the time of the treatment planning (2010), were the standard values used for tumors of the brain and head and neck at Mayo Clinic.

Priority 1	Pituitary mean dose < 36 Gy Lacrimal glands < 25 Gy Brainstem < 50 Gy or < 1% or < 1 cm^3 > 55 Gy Optic nerve/chiasm < 50 Gy or < 1% > 55 Gy Spinal cord < 45 Gy or < 1% or < 1 cm^3 > 50 Gy
Priority 2	>95% of the PTV to receive the prescribed dose <20% of the PTV to receive > 105% of the prescribed dose <1% of the PTV to get < 93% of the prescribed dose 1% or < 1 cm^3 of unspecified tissue outside of the PTV to receive > 105% of the prescribed dose
Priority 3	Parotids < 10 Gy
Priority 4	Oral cavity/lips/nasal cavity mean dose 20 Gy and < 1% > 40 Gy Inner/middle ear mean dose 30 Gy and < 1% > 50 Gy Eyes mean dose < 30 Gy and < 1% > 40 Gy Lens as low as reasonably possible

the postresection GTV (the small, irregularly shaped volume of visible tumor within the high-dose region corresponding to the CTV) being colored red in the surviving fraction maps in Fig. 4. Normal tissues have a greater capacity to repair radiation damage and therefore benefit from fractionated treatment schedules. Such tissues are therefore less affected than the tumor by the same radiation dose if delivered in daily fractions (as modeled here).

Figure 4 also shows a voxelized calculation of cells transformed for both the LQE and L models [Eqs. (7) and (8)] for a sagittal slice through the center of the GTV. The IMRT plan has the potential to induce transformed cells in a much larger volume of healthy tissue than the proton plan. This is because a much larger volume of healthy tissue receives low to intermediate doses. For the LQE model, both plans have a low probability of inducing transformed cells in the tumor region because the model accounts for sterilization and/or death of cells at high doses; hence, the probability of transformation tends to zero as dose tends to infinity. For the linear model, the risk of induction continues to increase with dose, and therefore, the high-dose regions are associated with the highest values of C_{TS}.

3.B. Integrated second cancer risk calculation

As described in Sec. 2.C.2, the expected number of cells transformed in each voxel can be summed to give the expected number of radiation-induced transformed cells in the entire treatment volume. The MIP distribution (the probability of ≥1 surviving transformed cells) is calculated for all four treatment plans for both models. The mean of these distributions can be interpreted as the average risk per patient expected in an irradiated cohort. The mean RelMIP values, corresponding to mean input parameters, are detailed in Table IV. While Tumor Control Probability (TCP) is comparable for all modalities, calculations of malignant induction shows that the mean $\text{RelMIP}_{\text{LQE}}$ is (normalized to the 3D conformal radiotherapy plan) 113% for volumetric modulated arc therapy, 16% for scanned protons, and 52% for intensity-modulated x-ray therapy. The mean RelMIP_{L} is 105% for volumetric modulated arc therapy, 42% for scanned protons, and 78% for intensity-modulated x-ray therapy.

The rank of the plans in terms of RelMIP is the same whether the linear or LQE induction probabilities are employed despite the large differences in these models, particularly in the behavior at high doses. All plans have very similar dose–volume characteristics in the tumor region (as prescribed), so the number of transformed cells in this volume is essentially independent of modality. Variation in RelMIP therefore arises due to differences in collateral irradiation outside the PTV, which occurs at low to moderate radiotherapy doses. In this low-dose region, for most tissues types, both the linear and LQE models predict an increasing probability of cell initiation as dose increases (with the linear model rising more rapidly as it is not being modified by the probability of survival). Therefore, the greater the volume of nontarget tissue receiving low to moderate dose, the larger the MIP.

3.C. Sensitivity of MIP to parameter uncertainty

The job management database was used to run the code 1000 times for each of the four treatment plans, where each run corresponds to a unique parameter set generated in a Monte Carlo fashion. Figure 5 shows the resulting distributions of MIP_{LQE} and $\text{RelMIP}_{\text{LQE}}$ from these calculations. The corresponding values for variance and mean for each plan are given in Table IV.

For each treatment plan and model, histograms can be produced displaying the distribution of MIPs [Eq. (9)] calculated for the range of parameter sets. There is an appreciable spread in the absolute MIP_{LQE} results, as illustrated in Fig. 5. In the case of 3DCFRT and VMAT, these distributions overlap, making it difficult to rank them in terms of MIP. Clearly, if the uncertainty spread on the input parameters had been even larger, so too would the uncertainty on the MIP distribution, making it even more difficult to rank the plans robustly.

TABLE II. A dosimetric summary of the four treatment plans detailing minimum, maximum, integral (int), mean (μ), and standard deviation (σ) doses within the volume enclosed by each contoured structure. Proton dose: D_{RBE} Gy(RBE) = RBE × D(Gy), where RBE is assumed to be 1.1 in every voxel.

		3DCFRT (Gy)				IMRT Dose (Gy)				VMAT Dose (Gy)				Proton Dose [Gy(RBE)]				
Structure	Volume (cm^3)	Min	Max	Int (GyL)	μ	σ	Min	Max	Int (GyL)	μ	σ	Min	Max	Int (GyL)	μ	σ	Min	Max	Int [Gy(RBE)L]	μ	σ
Soft tissue	2336.7	0.0	53.1	3.4	1.5	3.4	0.0	55	1.6	0.7	3.3	0	54.6	4.0	1.7	3.7	0.0	53.5	0.9	0.4	3
Brain	1441.6	0.6	52.9	13.3	9.2	12.4	0.0	56	10.7	7.4	12.2	0.2	55	14.7	10.2	11.9	0.0	53.6	6.1	4.2	11.7
Bone	1295.9	0.0	53.5	5.4	4.2	8.2	0.0	55.3	4.4	3.4	8.3	0.0	55.2	5.3	4.1	7.6	0.0	53.9	2.5	1.9	7.5
PTV	47.5	44.6	53.5	2.5	51.9	0.8	40.8	56.0	2.5	52.0	2.1	44.2	55.2	2.5	51.9	1.0	46.6	53.9	2.5	51.6	0.7
Lips, nasal, and oral cavities	31.3	0.8	32.7	0.1	2.3	3.1	0.3	35.9	0.3	10.5	7.3	0.5	43.3	0.2	5.0	6.7	0.0	34.6	0.0	1.1	4.0
Brainstem	29.3	2.5	52.8	1.0	34.3	15.3	1.3	50.5	1.0	33.8	13.2	5.8	54.4	1.0	33.5	13.2	0.0	52.8	0.8	28.4	19.3
All other tissues	4625.1	0.0	53.0	9.3	2.0	4.7	0.0	53.5	6.9	1.5	5.1	0.0	53.4	9.3	2.0	4.2	0.0	52.4	3.2	0.7	4.1

Relative MIP is defined in Sec. 2.C.2 as the ratio of a particular plan's MIP to that calculated for a reference plan on the same patient with the same radiobiological parameter set. In Fig. 5, 3DCFRT is used as the reference plan. As with absolute MIP, a variation in relative MIP is seen for the range of parameter sets, but the relative widths of the distributions are greatly reduced. This is because the MIP of each plan responds in a similar way to changes in parameters, and therefore, some of the input parameter-based uncertainty effectively "cancels out" when calculating the ratio. It should be noted that similar distributions were produced for MIP_L and that the plan ranking remained the same (see Table IV). Percentage uncertainties on relative MIP are notably even smaller in this case, because the linearity of the dose–response model guarantees that an increase in input parameter will result in an increase in MIP of both plans and vice versa.

The reduction in uncertainty is greatest when plans are similar in terms of dose distribution. Hence, it is possible to quote the relative MIP for the IMRT or VMAT treatments compared to the 3DCFRT technique with higher precision than the proton plan. The proton relative MIP distribution is somewhat broader than the photon distributions because the more different the plan is, in terms of dose–volume characteristics to the reference plan, the less the uncertainties in the radiobiological parameters cancel when the ratio is calculated.

The features described in this section have demonstrated that relative MIP is a robust metric for ranking plans, despite uncertainties in the radiobiological model and parameters that are most appropriate for predicting cancer induction.

4. DISCUSSION

Radiotherapy is a long established technology, with a large epidemiological knowledge base. Many protocols for producing treatment plans have been designed and refined over its history. As newer treatment modalities become more widely available, it is important for clinical staff to be able to compare new treatment plans with established protocols in a clinically meaningful way. Relative MIP may become a useful index for plan comparison, making it easier for clinicians to evaluate the potential improvements or hazards of implementing new treatment techniques.

The software presented here is designed to act as an additional tool in treatment planning, working from the dose distribution data produced by the clinical treatment planning system. There may, therefore, be additional risk factors not considered in our analysis. Treatment planning systems do not typically model radiation dose that is a long way out-of-field. The impact of low-dose irradiation is highlighted in this example by a positive shift in the distribution of MIP for 3DCFRT and VMAT treatment plans compared to the IMRT and proton plans, as a result of noncoplanar beams that deliver additional low doses of radiotherapy to the body inferior to the cranium and far from the PTV. These low doses would be considered trivial in the course of clinical treatment planning today, where the focus is mainly on causal acute and late

TABLE III. Mean (denoted by a superscript bar) radiobiological parameters used to calculate the expected number of surviving transformed cells in each voxel of the meningioma treatment plans. α and β are the linear–quadratic cell-kill parameters, γ and δ are the corresponding parameters for cell transformation. Parameter values chosen are taken to represent average values during a treatment course. The initial cell density for all tissues is $10^8/\text{cm}^3$.

Tissue type	Relevant contours	$\bar{\alpha}$ (Gy^{-1})[a]	$\bar{\beta}$ (Gy^{-2})	$\bar{\gamma}$ (Gy^{-1})	$\bar{\delta}$ (Gy^{-2})
Brain in GTV and CTV	CTV, GTV	0.060	0.0300	6.00×10^{-8}	3.00×10^{-8}
Brain and nerve tissue	Brain, PTV–CTV margin, brainstem, optic chiasm, optic nerves	0.060	0.0300	6.00×10^{-8}	3.00×10^{-8}
Bone	Bone	0.069	0.0300	6.90×10^{-8}	3.00×10^{-8}
Mucosal tissues	Lips, nasal, and oral cavities	0.300	0.0300	3.00×10^{-7}	3.00×10^{-8}
Other tissues	Ears, eyes, lacrimal glands, parotid glands, pituitary gland, soft tissue, patient	0.090	0.0300	9.00×10^{-8}	3.00×10^{-8}
Meningioma	GTV	0.150	0.0399		

[a]The illustrative $\bar{\gamma}$ values used give lower transformation probabilities than typically observed *in-vitro* (Ref. 23) and are approximately an order of magnitude lower than the example value given by Sachs and Brenner (Ref. 10) and an order of magnitude higher than values used in an earlier 2D geometric study (Ref. 31).

radiation injury, but the MIP model emphasizes the potential impact of such beam choices.

The quantitative analysis that has been carried out compares two models for induction (linear and LQE). These do not account for every possible dose–response curve in the literature but, with the appropriate calibration of parameters, most models (e.g., plateau models) fall somewhere between these limiting cases. Only induction has been simulated under the assumption that promotion and progression are independent of radiation and do not need to be considered when comparing

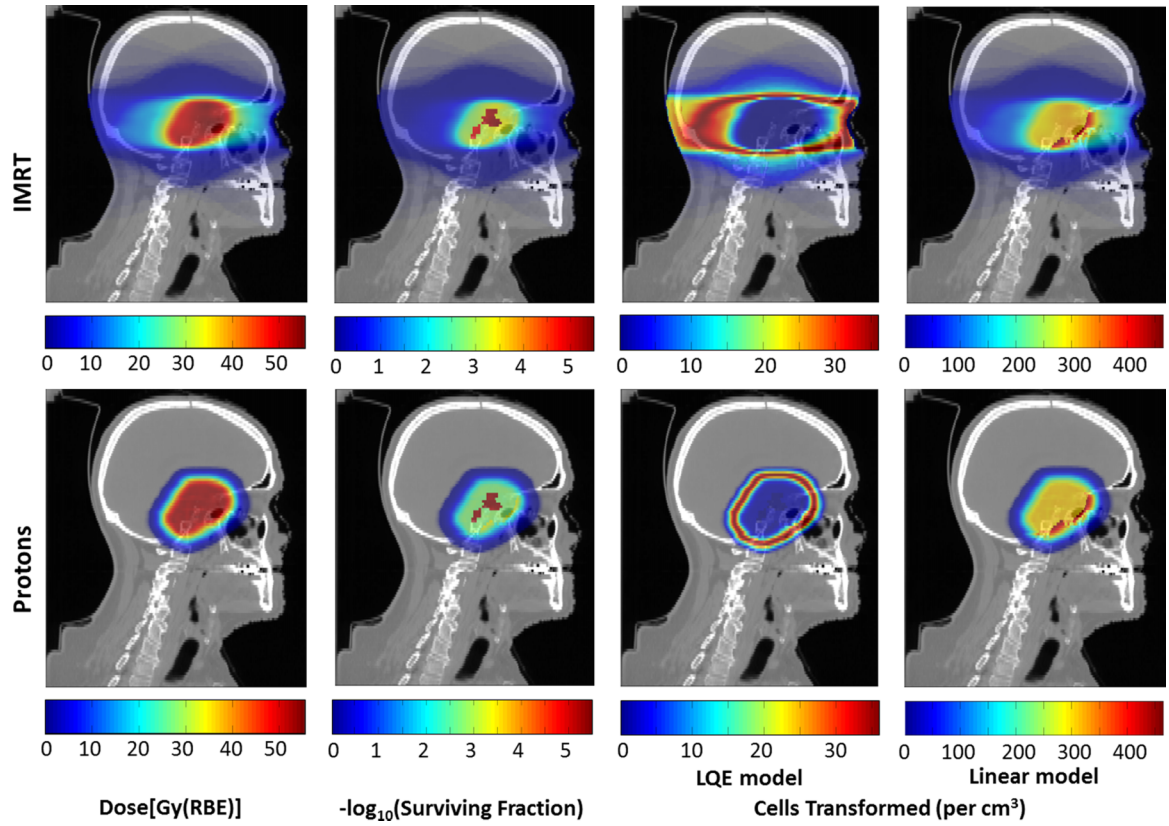

FIG. 4. 2D maps of dose, surviving fraction, and expected number of cells transformed [for both the LQE model and the linear (L) model] in the intensity-modulated x-ray and proton treatments of a subtotally resected meningioma. Note that the transformed cell densities apply to radiation-induced premalignant cell damage, which is much more prevalent than observed clinical malignancies, and the color bars for LQE and L models have different scales. The maps shown are sagittal slices through the centre of the GTV and the color washes fade out for doses lower than 1% of maximum dose. RBE = 1.1 for the proton plan and 1.0 for the IMRT plan.

TABLE IV. Tumor Control Probability (TCP) and relative malignant induction probability ($RelMIP_{LQE}$ and $RelMIP_{L}$) statistics for calculations using 1000 different radiobiological parameter sets. For TCP, the resulting distribution is skewed and so median is reported together with the positions of the first and third quartiles. The variability in absolute MIP is demonstrated by quoting the coefficient of variation (σ/μ). For relative MIP, mean and standard deviation are reported.

		Linear–quadratic–exponential model			Linear model		
Treatment Plan	TCP (%)	σ/μ (%) for MIP	RelMIP	σ/μ (%) for RelMIP	σ/μ (%) for MIP	RelMIP	σ/μ (%) for RelMIP
3DCFRT	$95.2^{+2.1}_{-3.6}$	10.0	1.0	0.0	9.0	1.0	0.0
IMRT	$95.9^{+1.8}_{-3.2}$	11.0	0.52 ± 0.01	2.1	9.2	0.78 ± 0.00	0.3
Protons	$94.4^{+2.4}_{-4.2}$	13.2	0.16 ± 0.01	5.1	9.6	0.42 ± 0.00	0.7
VMAT	$94.4^{+2.4}_{-4.1}$	9.8	1.13 ± 0.00	0.4	8.9	1.05 ± 0.00	0.2

plans on the same patient. There are further reasons why the calculated maps of transformed cells *in-vivo* (shown in Fig. 4) may not agree with the actual cancer incidence in 3D. For example, if ϵ is not the same for every voxel in the treatment volume, due to the fact that different anatomical regions have a promotion and/or progression advantage over others, then a cell initiated in one region of the treatment volume could be more likely to become an overt malignancy than a cell in another. This effect would need to be explicitly modeled in order to bridge the gap between initiation of premalignant cells and induced cancers. Likewise, an explicit incorporation of repopulation in the LQE model can show a plateau-shaped dose–response curve,[21] which would lead to an elevated cancer risk in the high-dose region. This software will be adapted to incorporate further models of second cancer induction, the validation of which will be aided by emerging clinical

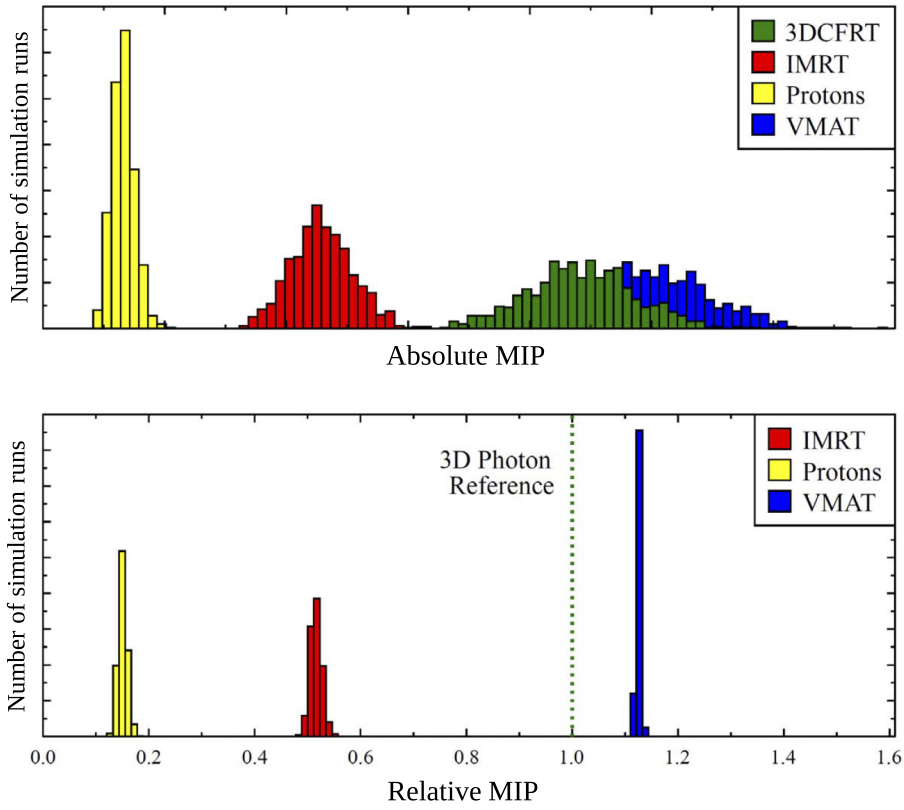

FIG. 5. Comparison of absolute and relative distributions of MIP_{LQE} for each treatment plan. The top figure shows absolute MIP_{LQE} distributions, which have a large spread relative to their mean values due to the input parameter uncertainties detailed in Fig. 3. The distributions for 3DCFRT and VMAT overlap, making it difficult to rank them in terms of MIP. No values are given for the absolute data as precise values would require calibration with clinical data, if available, which is beyond the scope of this study. The bottom figure shows the distribution of the three modalities normalized against the 3DCFRT baseline. When these ratios are used for each given sample parameter set, the distributions become much narrower, allowing the plans to be more clearly distinguished. Note that normalizing the 3DCFRT plan to itself, for each parameter set, leads to a single bin of size 1000 at relative MIP = 1 so this bin has been replaced with a dotted line at 1 to indicate the reference point.

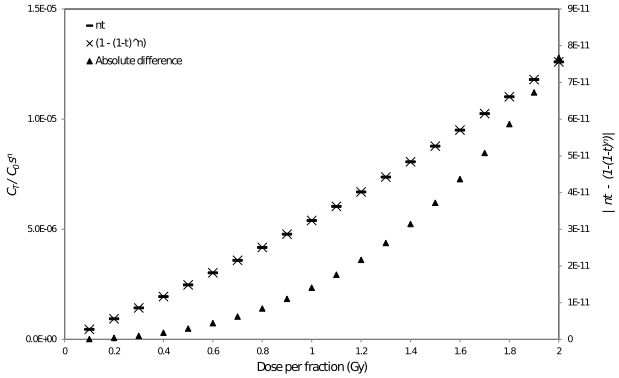

FIG. 6. Graph showing $[1-(1-t)^n]$ and the first term in the expansion nt for clinically relevant values for the parameters α, β, γ, δ, and n. It shows that the absolute difference between the full equation and the approximation is less than 10^{-10} (4–5 orders of magnitude smaller than the value itself) for the dose range of interest, and therefore, it is considered appropriate to use the approximation nt in the simulation.

data. There is also no consideration of the fact that delivered dose may well vary from the planned dose. For the proton treatment plan, the RBE is assumed to be 1.1 throughout the treatment volume, which is clearly an approximation. The software has been designed in a flexible way such that it can incorporate variable RBE models to account for dependence on LET, α/β, and dose per fraction, if appropriate Monte Carlo planning data are available. In addition, it should be noted that the proton plan used in this paper is actively scanned and therefore associated with low neutron dose.[36] However, with large uncertainties in the biological effect of neutrons at different energies, it may still be necessary to take neutron induced MIP into account. The authors note the work of the ADANTE Consortium[37] in this respect and plan to incorporate neutron MIP models, when available, to quantify this effect. With passively scattered proton plans, there would be a potentially relevant MIP from the externally produced neutrons which would also need to be considered.

Further work is ongoing to extend this analysis to other cancer sites. It is of particular interest for the treatment of tumors in sites for which avoidance of long-term side effects, such as MIP, may be particularly important, e.g., pediatric medulloblastoma. It may be informative to use this method to calculate MIP on a per organ basis for Hodgkin's patients, for example, and compare to the results produced using the organ equivalent dose concept.[22]

Irradiation may substantially deplete the level of tumor and normal tissue cells leading to replenishment via repopulation. Some repopulation effects, especially in human tumors, can be appreciable. The LQE model used here does not include repopulation, while the linear model is a limiting case of models that do. It is part of ongoing work to incorporate repopulation explicitly, which would need to include different lag times and proliferation rates for different tissue types.

These results show that relative MIP is much less sensitive to variations in radiobiological parameters than any absolute prediction of risk, so it may be acceptable to simply use mean values to calculate accurate relative MIP. Having said that it would be necessary, preferably from clinical data if available, to have a reasonable estimate for absolute risk. If this risk is negligibly small it could be argued that even 84% reduction in risk (as shown here in the comparison between proton and conventional treatments) may be considered irrelevant. Equally, if the expected survival time is short, then an elevated risk of cancer more than 10 yr post-treatment may not be a useful metric to base treatment choice upon.

5. CONCLUSION

As secondary tumorigenesis becomes a more relevant component of radiotherapy planning, and the variety of treatment modalities available to the treating clinician increase, it will be more and more important to select treatment plans on the basis of their relative MIP values. This paper has demonstrated a novel tool for MIP calculation following radiotherapy which incorporates the heterogeneous response of tissues to radiation and patient-specific dose. Explicit treatment of parameter uncertainties has enabled quantification of the corresponding uncertainty in the MIP estimate. It has been shown that plans can be distinguished by their relative secondary tumor risks more reliably, even when the absolute probabilities are comparatively uncertain.

APPENDIX: DERIVATION OF FRACTIONATED MIP FORMULA

Referring to Fig. 1, it can be see that for an arbitrary number of fractions, n, the expected number of transformed cells will be given by

$$C_{TS}(n,d) = C_0 P_{TS}(n,d) = C_0 s^n t(1+(1-t)+(1-t)^2+\cdots+(1-t)^{n-1}). \quad \text{(A1)}$$

As only two classes of surviving cells are considered, the probability of a cell remaining untransformed given that it survives a fraction is simply $(1-t)$. Equation (A1) is a geometric progression with first term $C_0 s^n t$ common ratio $(1-t)$ and terms n. It can thus be simplified to

$$C_{TS} = C_0 s^n t\left(\frac{1-(1-t)^n}{t}\right) = C_0 s^n (1-(1-t)^n). \quad \text{(A2)}$$

The linear–quadratic cell-kill model provides the substitution $s = e^{-(\alpha d+\beta d^2)}$,

$$C_{TS} = C_0 e^{-n(\alpha d+\beta d^2)}(1-(1-t)^n). \quad \text{(A3)}$$

In the limit that t is much smaller than 1, $C_{TS} \approx C_0 e^{-n(\alpha d+\beta d^2)} nt$ as shown in Fig. 6.

[a]Author to whom correspondence should be addressed. Electronic mail: claire.timlin@ptcri.ox.ac.uk

[1]E. J. Hall and C.-S. Wuu, "Radiation-induced second cancers: The impact of 3D-CRT and IMRT," Int. J. Radiat. Oncol., Biol., Phys. **56**, 83–88 (2003).
[2]I. Shuryak, P. Hahnfeldt, L. Hlatky, R. K. Sachs, and D. J. Brenner, "A new view of radiation-induced cancer: Integrating short- and long-term processes. Part II: Second cancer risk estimation," Radiat. Environ. Biophys. **48**, 275–286 (2009).

[3]M. P. Coleman, D. Forman, H. Bryant, J. Butler, B. Rachet, C. Maringe, U. Nur, E. Tracey, M. Coory, J. Hatcher, C. E. McGahan, D. Turner, L. Marrett, M. L. Gjerstorff, T. B. Johannesen, J. Adolfsson, M. Lambe, G. Lawrence, D. Meechan, E. J. Morris, R. Middleton, J. Steward, and M. A. Richards, "Cancer survival in Australia, Canada, Denmark, Norway, Sweden, and the UK, 1995–2007 (the International Cancer Benchmarking Partnership): An analysis of population-based cancer registry data," Lancet **377**, 127–138 (2011).
[4]P. Vineis, A. Schatzkin, and J. D. Potter, "Models of carcinogenesis: An overview," Carcinogenesis **31**, 1703–1709 (2010).
[5]H. Hennings, A. B. Glick, D. A. Greenhalgh, D. L. Morgan, J. E. Strickland, T. Tennenbaum, and S. H Yuspa, "Critical aspects of initiation, promotion, and progression in multistage epidermal carcinogenesis," Exp. Biol. Med. **202**(1), 1–8 (1993).
[6]T. L. Vincent and R. A. Gatenby, "An evolutionary model for initiation, promotion, and progression in carcinogenesis," Int. J. Oncol. **32**, 729–737 (2008).
[7]S. H. Moolgavkar, "Model for human carcinogenesis—Action of environmental agents," Environ. Health Perspect. **50**, 285–291 (1983).
[8]D. D. Hanahan and R. A. R. Weinberg, "The hallmarks of cancer," Cell **100**, 57–70 (2000).
[9]M. P. Little, W. F. Heidenreich, S. H. Moolgavkar, H. Schöllnberger, and D. C. Thomas, "Systems biological and mechanistic modelling of radiation-induced cancer," Radiat. Environ. Biophys. **47**, 39–47 (2007).
[10]R. K. Sachs and D. J. Brenner, "Solid tumor risks after high doses of ionizing radiation," Proc. Natl. Acad. Sci U. S. A **102**, 13040–13045 (2005).
[11]U. Schneider, "Modeling the risk of secondary malignancies after radiotherapy," Genes **2**, 1033–1049 (2011).
[12]E. J. Hall, "The crooked shall be made straight; dose–response relationships for carcinogenesis," Int. J. Radiat. Biol. **80**, 327–337 (2004).
[13]H. Suit, S. Goldberg, A. Niemierko, M. Ancukiewicz, E. Hall, M. Goitein, W. Wong, and H. Paganetti, "Secondary carcinogenesis in patients treated with radiation: A review of data on radiation-induced cancers in human, non-human primate, canine and rodent subjects," Radiat. Res. **167**(1), 12–42 (2007).
[14]X. G. Xu, B. Bednarz, and H. Paganetti, "A review of dosimetry studies on external-beam radiation treatment with respect to second cancer induction," Phys. Med. Biol. **53**, R193–R241 (2008).
[15]BEIR (National Research Council, National Academy of Science), Health risks from exposure to low levels of ionizing radiation, *BEIR VII, Phase 2*, 2006.
[16]M. Tubiana, "Can we reduce the incidence of second primary malignancies occurring after radiotherapy? A critical review," Radiother. Oncol. **91**(1), 4–15 (2009).
[17]A. B. de Gonzalez, E. Gilbert, R. Curtis, P. Inskip, R. Kleinerman, L. Morton, P. Rajaraman, and M. P. Little, "Second solid cancers after radiation therapy: A systematic review of the epidemiologic studies of the radiation dose–response relationship," Int. J. Radiat. Oncol., Biol., Phys. **86**(2), 224–233 (2013).
[18]P. Bhatti *et al.*, "Risk of second primary thyroid cancer after radiotherapy for a childhood cancer in a large cohort study: An update from the childhood cancer survivor study," Radiat. Res. **174**(6), 741–752 (2010).
[19]S. Sakasi and N. Fukuda, "Dose-response relationship for induction of solid tumors in female B6C3F1 mice irradiated neonatally with a single dose of gamma rays," J. Radiat. Res. **40**(3), 229–241 (1999).
[20]L. H. Gray, *Cellular Radiation Biology* (Williams and Wilkens, Baltimore, 1965).
[21]R. K. Sachs, I. Shuryak, D. Brenner, H. Fakir, L. Hlatky, and P. Hahnfeldtd, "Second cancers after fractionated radiotherapy: Stochastic population dynamics effects," J. Theor. Biol. **249**(3), 518–531 (2007).
[22]U. Schneider, D. Zwahlen, D. Ross, and B. Kaser-Hotz, "Estimation of radiation-induced cancer from three-dimensional dose distributions: Concept of organ equivalent dose," Int. J. Radiat. Oncol., Biol., Phys. **61**, 1510–1515 (2005).
[23]UNSCEAR, UNSCEAR 1986 Report: Genetic and Somatic Effects of Ionizing Radiation, Annex B: Dose–response Relationships for Radiation-induced Cancer, 1986, pp. 165–206.
[24]B. Jones, "Modelling carcinogenesis after radiotherapy using Poisson statistics: Implications for IMRT, protons and ions," J. Radiol. Prot. **29**(2A), A143–A157 (2009).
[25]A. Daşu *et al.*, "The use of risk estimation models for the induction of secondary cancers following radiotherapy," Acta Oncol. **44**, 339–347 (2005).
[26]R. M. Harrison, "Second cancers following radiotherapy: A suggested common dosimetry framework for therapeutic and concomitant exposures," Br. J. Radiol. **77**, 986–990 (2004).
[27]ICRP, Low-dose Extrapolation of Radiation-related Cancer Risk, ICRP Publication 99, 2005.
[28]K. Ozasa, Y. Shimizu, A. Suyama, F. Kasagi, M. Soda, E. J. Grant, R. Sakata, H. Sugiyama, and K. Kodama, "Studies of the mortality of atomic bomb survivors, Report 14, 1950–2003: An overview of cancer and noncancer diseases," Radiat. Res. **177**, 229–243 (2012).
[29]MATLAB version R2010a, The Mathworks, Inc., Natick, MA, 2010.
[30]J. O. Deasy, A. I. Blanco, and V. H. Clark, "CERR: A computational environment for radiotherapy research," Med. Phys. **30**, 979–985 (2003).
[31]C. Timlin, M. Houston, and B. Jones, "Malignant induction probability maps for radiotherapy using x-ray and proton beams," Br. J. Radiol. **84**, S70–S78 (2011).
[32]*Basic Clinical Radiobiology*, 3rd ed., edited by G. G. Steel (Hodder Education, London, UK, 2002).
[33]F. J. Vernimmen and J. P. Slabbert, "Assessment of the alpha/beta ratios for arteriovenous malformations, meningiomas, acoustic neuromas, and the optic chiasma," Int. J. Radiat. Biol. **86**, 486–498 (2010).
[34]P. Strojan, "Secondary intracranial meningiomas after high-dose cranial irradiation: Report of five cases and review of the literature," Int. J. Radiat. Oncol., Biol., Phys. **48**, 65–73 (2000).
[35]G. Minniti, D. Traish, S. Ashley, A. Gonsalves, and M. Brada, "Risk of second brain tumor after conservative surgery and radiotherapy for pituitary adenoma: Update after an additional 10 years," J. Clin. Endocrinol. Metab. **90**(2), 800–804 (2005).
[36]U. Schneider, S. Agosteo, E. Pedroni, and J. Besserer, "Secondary neutron dose during proton therapy using spot scanning," Int. J. Radiat. Oncol., Biol., Phys. **53**, 244–251 (2001).
[37]http://www.andanteproject.eu/, Andante Consortium, 2012.